Cross-Axis Flexural Pivots in Mechatronic Applications: Stress-Based Design for Combined Tension and Bending

Brandon T. Peterson, *Member, IEEE*, Thomas J. Hardin, Armin W. Pomeroy, Jonathan B. Hopkins, *Member, IEEE*, and Tyler R. Clites

***Abstract*—Cross-axis flexural pivots (x-pivots) hold immense promise as precise, frictionless bearing elements in mechatronic systems. In real-world settings, where bearings are called upon to bear nontrivial loads orthogonal to the axis of rotation, kinematic and stiffness-based design approaches are insufficient to ensure longevity. Stress-based design, which is the norm in conventional rolling- or sliding-contact bearing selection, allows for direct calculation of expected fatigue lifetime, as well as performance in acute overload scenarios. However, the principles that guide stress-based design for flexural bearings are distinct from those that govern contact bearings, and have not yet been clearly described. In this article, we present three physical principles that came to light as we applied stress-oriented finite element analysis to design x-pivots for large angular deformation and heavy tensile loads. Specifically, we describe cross-blade anticlastic effects, loading scenarios that can lead to buckling when the mechanism is in tension, and nonlinear stress effects that emerge in combined tension and bending. These principles have an outsized impact on the mechanism's stress profile, and are not well represented in existing x-pivot models. We also discuss ways to leverage gross mechanism geometry and blade profile to mitigate or avoid these effects. We expect that this work will help facilitate the design of x-pivots for applications in real-world mechatronic systems.**

***Index Terms*—Compliant mechanisms, cross-axis flexural pivots, stress-based design.**

Manuscript received 23 February 2023; revised 27 June 2023 and 1 November 2023; accepted 8 November 2023. Date of publication 5 December 2023; date of current version 18 April 2024. Recommended by Technical Editor G. Berselli and Senior Editor G. Berselli. This work was supported by the David Geffen School of Medicine Seed Grant. This article has been authored by an employee of National Technology & Engineering Solutions of Sandia, LLC under Grant DE-NA0003525 with the U.S. Department of Energy. *(Brandon T. Peterson and Thomas J. Hardin contributed equally to this work.) (Corresponding author: Tyler R. Clites.)*

Brandon T. Peterson, Armin W. Pomeroy, and Jonathan B. Hopkins are with the Department of Mechanical and Aerospace Engineering, University of California Los Angeles, Los Angeles, CA 90095 USA (e-mail: peachpeterson@ucla.edu; arminpomeroy@g.ucla.edu; hopkins@seas.ucla.edu).

Thomas J. Hardin is with the Material, Physical, and Chemical Sciences Center, Sandia National Laboratories, Albuquerque, NM 87123 USA (e-mail: tjhardi@sandia.gov).

Tyler R. Clites is with the Department of Mechanical and Aerospace Engineering and Orthopaedic Surgery, University of California Los Angeles, Los Angeles, CA 90095 USA (e-mail: clites@ucla.edu).

This article has supplementary material provided by the authors and color versions of one or more figures available at https://doi.org/10.1109/TMECH.2023.3334994.

Digital Object Identifier 10.1109/TMECH.2023.3334994

I. Introduction

COMPLIANT mechanisms have the potential to precisely guide motion with little or no friction and negligible wear [1], [2], [3], [4], [5], [6], [7], [8], [9], [10]. From the litany of potential mechanism designs that constrain motion in all degrees of freedom except a single axis of rotation [2], [3], [4], the cross-axis flexural pivot (x-pivot), [see Fig. 1(a)] [11], [12] is uniquely able to achieve large angular displacement with relatively little parasitic motion [13], [14], [15], [16], [17], [18]. X-pivots also stand out in their ability to withstand large uniaxial loads in tension or, if the mechanism is inverted, in compression [13], [19].

Part of the promise of x-pivots is their potential to replace conventional contact bearings in real-world mechatronic applications, thereby eliminating friction and wear-based failure. To realize this promise, it will be essential to develop flexural elements that perform well under specific combinations of non-negligible angular displacement and uniaxial load. In keeping with established machine design principles for bearings [20], [21], [22], the design process for a flexural bearing would primarily emphasize cycles-to-failure and load-to-failure calculations. For compliant mechanisms, these calculations are built from estimation of the peak stress within the device during anticipated loads, and comparison of that stress to the material's fatigue or yield stress. In working through this design process for x-pivots, we recently came to understand a few key principles that play a nontrivial role in mechanism performance, are not well captured in existing models, and are currently absent in the published literature. The purpose of this article is to share those principles with the community, so that others seeking to design x-pivots for real-world mechatronic systems have a sense for what to expect.

II. Methods

A. Existing Models

As a starting point in our design process, we first sought analytical models to gain intuition for the fundamental principles

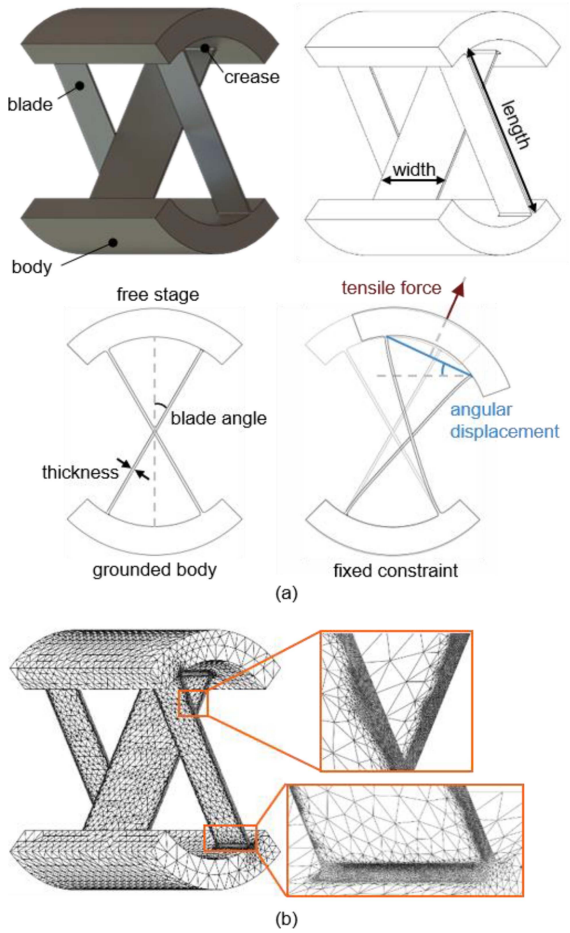

Fig. 1. (a) Schematic of the symmetric three-blade x-pivot used for simulation, showing principal geometric parameters and finite element analysis (FEA) setup. (b) Representative mesh after three iterations of adaptive meshing. Higher density meshes were generated across the blade thickness and at the creases.

that guide x-pivot performance. Fortunately, an extensive analytical foundation has been established in previous works to understand the angular force-displacement behavior of x-pivots [23], [24], [25], [26], [27]. This emphasis on rotational compliance is appropriate: passive mechanics are fundamental to compliant mechanism design and tend to be well represented in simplified models and well verified experimentally. Rotational compliance alone is not sufficient to predict fatigue lifetime, which is crucial to applications involving bearing elements that are repeatedly loaded. An understanding of the stresses generated from the applied loads can help ensure mechanism longevity and protect from overload scenarios.

In only a few cases, these stiffness models have been extended to predict maximum stress within an x-pivot's angled blades. In the simplest of these models, Jensen and Howell [23] consider mechanism angular displacement in the absence of tension; the blades are modeled as independent beam elements in pure bending, constrained to a fixed value of angular deformation at their ends. The maximum stress in these beams is estimated using Euler–Bernoulli beam theory, and that classical bending stress is then multiplied by an empirical scale factor such that the analytical values closely match those derived from finite element analysis (FEA). This provides an analytical model for stress as a function of mechanism angular displacement that generalizes well across x-pivot geometries. In a separate publication, Guérinot et al. [19] propose a simple analytical model to predict stress in each blade from pure tensile load on the mechanism (absent mechanism angular displacement). In a later review of this work, Ma et al. [28] posited that the predictions from these two models could be summed linearly to provide a first-order approximation for combined loading in both angular displacement and tension. However, the accuracy of this approximation neglects nonlinear interactions between the tension and angular displacement, which we have found to be non-negligible (see Section III-C for more detail). Guérinot's model also assumes that the loading vector is parallel to the blade bisector, and therefore does not capture the dependency of blade stress on tensile loading direction (see Section III-B).

In a more recent model, Ma et al. [28] presented a 2-D finite-element-like model of the x-pivot, in which each blade is modeled as a chain of 1-D discrete "beamlet" elements. Using this model, it is possible to calculate a global mechanism stiffness, as well as a local stress distribution in each beamlet when the complete mechanism is subjected to any combination of rotational and tensile loads. However, Ma's model does not account for stress variations across the width of the blade, which we have found to be non-trivial (see *Anticlastic Curvature*). In addition, Ma's 1-D beams do not allow for modeling of non-constant beam geometries (as formulated in [28], though we suspect this limitation could be readily overcome), which we have found play a crucial role in reducing or eliminating stress concentrations (see Section III-C).

The Bi-beam constraint model [25] combines many of the strengths of Euler–Bernoulli beam-based analysis and Ma's discretization approach by considering each blade of the x-pivot in terms of two linked variable-profile beams. In addition to enabling analysis of polynomial blade profiles, this approach increased accuracy of predictions at large angular deflections, and was applied to a specific cable-actuated loading scenario. However, as a 2-D model, this approach necessarily neglects cross-width stress variation.

Limitations of the existing models became apparent once we began running 3-D FEA simulations to spot-check our design work in the context of general combined loading, which began with these lower order models. Upon seeing major discrepancies between the lower order and 3-D FEA predictions, we sought to understand the physical causes and implications of these discrepancies.

B. Finite Element Analysis Setup

All 3-D FEA for this study was performed in Abaqus (Dassault Systems, 2020). A symmetric three-blade x-pivot mechanism was constructed in SolidWorks (Dassault Systems, 2020) for FEA testing, consisting of a grounded body and a free stage, connected by the x-pivot blades [see Fig. 1(a)]. A three-blade pivot was selected over the more conventional two-blade pivot to avoid off-axis parasitic motions that can emerge when an

asymmetric two-blade x-pivot is loaded in tension. The three blades span a total width of 4 cm [except for the analysis in Fig. 2(c), in which blade width varies], and are each 4 cm long. The outer blades (9.5 mm wide) are ½ the width of the inner blade (19 mm wide) such that the total blade width is shared equally across the two blade directions. A gap of 1 mm was included between each blade to prevent interference. A blade angle of 30° was used for all simulations.

For the width-thickness anticlastic curvature plots [see Fig. 2(c)], blade thickness was held constant at 0.85 mm; width-to-thickness ratio was altered by sweeping blade widths. This blade thickness was chosen to bring the mechanism close to yield stress at 30° of mechanism angular displacement. All other simulations used a blade thickness of 0.5 mm.

For all simulations and all blade types, 0.5 mm radius fillets were introduced at the blade-body creases (see Fig. 1) to smooth out stress concentrations. The simulations that illustrate anticlastic curvature [see Fig. 2(c)], buckling [see Fig. 3(c)], and stress concentrations [see Fig. 5(b) and (d)] all utilize x-pivots with blades of constant width and thickness (CWT), i.e., they include no additional fillet features aside from the universal crease fillets.

For the variable width (VW) simulations in Figs. 6 and 8, the inner blade was 22.8 mm wide at its base and 15.2 mm wide at its center. The outer blades were 15.2 mm wide at their bases and 7.6 mm wide at their centers. These dimensions were chosen to maintain a total mechanism width of 4 cm while overlapping the blade bases as much as possible (see Section IV-B for more detail). For the variable thickness (VT) blades, thickness at the base of each blade was 1.5 mm; this then tapered elliptically to the 0.5 mm blade thickness over a distance of 8 mm along the length of the blade. These taper parameters were chosen arbitrarily, but were checked against a range of other tapers to ensure that the results were representative of the impact of varying blade thickness. A summary of all blade parameters for each simulation and experiment is provided in the Supplementary materials.

Material properties for Titanium 6Al-4V were assigned across all simulations; this material was chosen based on its excellent strength-to-weight ratio and fatigue properties, which make it an exceptional candidate for compliant mechanisms. Each x-pivot "part" was meshed with an initial global seed spacing of 2 mm. This mesh was then densified at regions of higher von Mises stress using a three-iteration adaptive meshing process; as would be expected, this led to higher mesh density across the blade thickness and in transitional regions at the creases [see Fig. 1(b)].

During simulations, the bottom of the grounded body was assigned a zero-displacement constraint. The upper half of the free stage was assigned a rigid-body constraint, and tensile forces and/or prescribed angular displacements were applied to a reference point tied to that rigid body. For all cases of combined loading, both the angular displacement and tensile forces were applied simultaneously, in a single step with multiple nonlinear increments. Tensile loads were always applied normal to the top face of the free stage, and rotated with that stage during mechanism angular displacement (rotation). To facilitate plotting trends, the Abaqus Python interface was used to automate sweeps of varying loads or geometries. For the sake of reporting the most accurate peak stress results, we extracted the maximum value from the resultant set of integration points. When plotting stress distributions for our figures, we extrapolated results to each node and averaged across region boundaries.

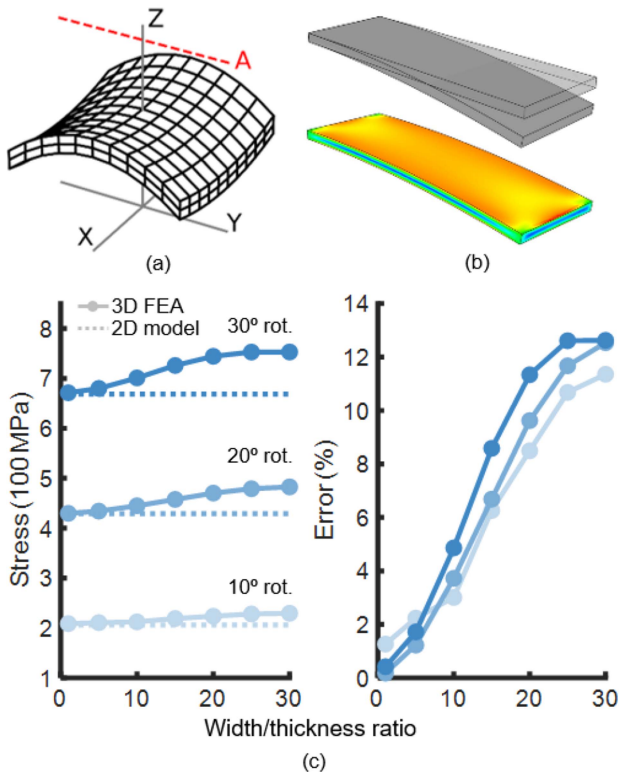

Fig. 2. (a) Representative cartoon of anticlastic effect on a thin plate. Relative deformations are exaggerated for illustrative purposes. (b) 3-D FEA showing a characteristic anticlastic stress profile in a wide cantilever beam in pure bending. Stress values are represented on a color spectrum from blue (low stress) to red (high stress). (c) Deviation in peak stress in the full x-pivot from [23] as a function of width-to-thickness ratio. Ratio is plotted as inner blade width divided by thickness. Thickness was held constant at 0.85 mm, and width was swept. Shades of blue represent amount of mechanism angular deformation (rotation). Error was calculated as (3-D FEA peak stress−2-D model peak stress)/2-D model peak stress x 100.

C. Experimental Validation

Benchtop experiments were conducted to further support the principles illustrated in Sections III-B and III-C. X-pivot mechanisms were 3-D-printed in micro carbon-fiber-filled nylon (Onyx, Markforged). Each mechanism had a total width of 4 cm, a blade length of 4 cm, and a blade angle of 30°. In the buckling experiment, CWT blade flexures of 4 mm thickness were bolted to a teststand in which one stage of the mechanism was grounded and the other was mounted to a serial robotic manipulator (KR-210, KUKA). The robot applied planar tensile loads of varying magnitude and angle while also providing a balancing torque to restrict rotation. The position of the stage was measured for various in-plane loads and loading angles. Buckling was identified as the onset of nonlinearity in the horizontal displacement of the stage as a function of loading angle, for several load magnitudes.

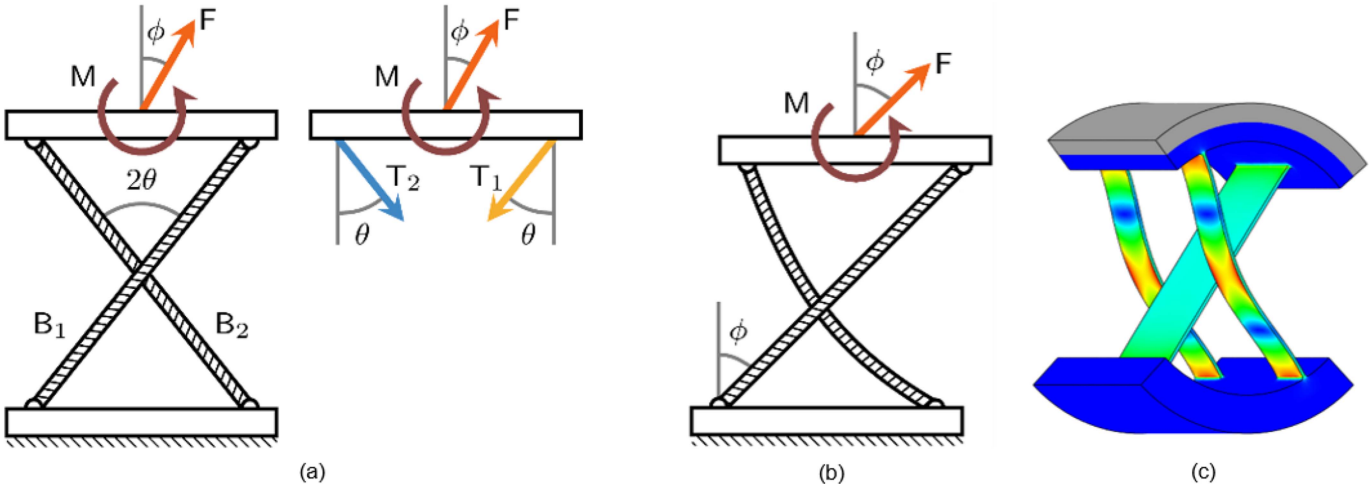

Fig. 3. (a) Illustrative model of the x-pivot as two bodies connected by crossing blade "ropes." (b) Schematic representation of how buckling can occur in one of the two blades while the whole mechanism is in tension. (c) FEA of the x-pivot in tension outside the blades, where the free stage is locked in rotation (M balances the moment from F), showing buckling in the outer blades. Stress values are represented on a color spectrum from blue (low stress) to red (high stress).

To experimentally validate our bowstringing observations, we compared the blade curvature under combined loading between a CWT blade x-pivot (0.5 mm thickness) and a VT blade x-pivot (1.5 mm base thickness tapered to 0.5 mm over a length of 10 mm). Both mechanisms were subjected to increasing tensile loads at a 30° angle, to pull the device into 30° of rotation. To achieve these loading conditions, one side of each mechanism was mounted in a vice at 30° relative to gravity, while weights were hung from the free stage. Image processing was used to estimate the radius of curvature at 1000 points along the blades under each loading scenario. The peak curvature for each blade and load was calculated as the maximum of the inverse of the radius of curvature at each point, multiplied by the blade length.

III. Challenges and Solutions in Stress-Based X-Pivot Design

A. Anticlastic Curvature

1) Problem: Anticlastic Curvature Produces Stress Variation Across Blade Width in Bending: The ability of the x-pivot to sustain a tensile load is, to first order, governed by the smallest cross-sectional area of the blade, sectioned perpendicular to the long axis of the blade. As such, the design requirements of compliance in bending (which requires a thin beam profile) and strength in tensile loading (requiring cross-sectional area) inevitably produce a wide, thin (plate-like) blade geometry. In contrast to beams, which are the typical element type used in modeling x-pivots, plates are known to undergo a parasitic deformation mode known as anticlastic curvature when loaded in bending. This effect has been understood for many years [29], but we have not found it mentioned in the literature in the context of compliant mechanisms.

Anticlastic curvature stems from the Poisson effect. Consider a thin plate initially parallel to and above the x–y plane, to which a moment is applied which bends the plate about the x-axis [see Fig. 2(a)]. The portion of the plate above the plate midplane experiences tension in the y-direction, while the portion of the plate below the midplane experiences compression in the y-direction. These stresses produce Poisson strain in the x-direction, with the plate expanding in x below the midplane and contracting in x above the midplane. This coupling of Poisson strains in the x-direction produces a parasitic net curvature of the plate about an axis above the plane and parallel to the y-axis [axis A in Fig. 2(a)], resulting in the plate assuming a net "saddle" shape. In the context of a cantilever beam, this appears in the stress field as an otherwise unexpected nonuniform stress across the width of the plate, characterized by bands of high stress along the plate edges [see Fig. 2(b)].

Anticlastic effects become important to stress-driven design of x-pivots as the aspect ratio of flexures becomes large (that is, as they become wide and thin). This is illustrated in Fig. 2(c), which shows that anticlastic deviations from existing 2-D models appear to level out around 13% error relative to 2-D model predictions [23], [28]. Notably, the stress concentrations associated with anticlastic effects are situated at the edges of the flexure, at prime locations for fatigue fracture nucleation [30].

2) Identifying and Addressing Unintended Anticlastic Curvature: Because the stresses associated with anticlastic curvature vary across the width of the plate, this phenomenon is not captured in models which homogenize stress across flexure width [31]. In other words, flexure blades with a large aspect ratio, when loaded at large angles, are prone to stress concentrations at blade edges that are not predicted by popular 2-D models. Therefore, in order to calculate the impact of anticlastic effects in a stress-driven design context, we recommend the use of 3-D finite element modeling, which does capture anticlastic effects.

We note also that the aspect ratio of x-pivot blades can be reduced (and, therefore, anticlastic effects can be reduced) without sacrificing cross-sectional surface area or increasing blade thickness, by increasing the number of blades in the x-pivot. However,

this approach raises significant manufacturability concerns (see Section IV-A).

To summarize, we view anticlastic curvature as a fact of life in the design space for x-pivots in bending. It is only dangerous when it is a surprise, and it is readily designed around in a stress-driven framework with the help of 3-D finite element modeling.

B. Buckling in Tension

1) Problem: Tensile Loading Can Induce Buckling Based on Loading Direction and Applied Moment: The x-pivot mechanism is a composite of flexible linear beam components joined by approximately rigid members. The stiffness of each of these beams in axial *tension* is the Young's modulus of the beam; however, because the beams are very thin relative to their length, they buckle under relatively low *compressive* axial loads. The thin beam geometry also implies that each beam also has low resistance to *bending* and *shear* loads. In other words, when only axial load is of interest at low device angular deflection, the blades of an x-pivot can be modeled in approximation as ropes that carry only tensile axial load.

Building from this analogy, we can model the x-pivot as two rigid body elements connected by intersecting ropes [see Fig. 3(a)]. Consider the scenario in which a moment M is applied in opposition to the moment created on the free stage by the force F. In the simplified case where these two moments are balanced, the rope system will reach static equilibrium; balancing the horizontal and vertical forces and solving for T_1 and T_2 returns

$$T_1 = F\, csc\,(2\theta)\ \sin\,(\theta - \phi) \tag{1}$$

$$T_2 = F\, csc\,(2\theta)\ \sin\,(\theta + \phi) \tag{2}$$

where $F > 0$, $\theta \in (0,\ \frac{\pi}{2})$ and $\phi \in [0,\ \frac{\pi}{2}]$. T_1 and T_2 are both nonnegative (that is, the ropes are not slack) precisely when ϕ falls inside of $[-\theta,\ \theta]$. When a symmetric x-pivot is undeformed, and the loading vector is aligned with the bisector of the two blade vectors [$\phi = 0$ in Fig. 3(a)], the reaction force is distributed symmetrically across the blades ($T_1 = T_2$). However, as the loading vector moves off of the bisector to instead be aligned more with one of the blade "ropes," we see an increase in T_1, the tension carried by B_1. This is a result of the ropes' inability to carry any load other than tension; as the resultant load on B_2 shifts to be oriented more transverse to the rope than axial, the balance of the reaction force shifts to B_1. As we can see in (1), this phenomenon causes T_1 to increase continuously with ϕ. This shift in tensile force becomes obvious in the extreme case: when $|\phi| = \theta$, B_2 is unable to contribute any tensile force ($T_2 = 0$), such that B_1 carries 100% of the reaction force ($T_1 = F$).

As the loading vector moves outside the blade vectors ($|\phi| > \theta$), T_2 becomes negative, which implies that B_2 is called upon to support a compressive load. This can be conceptualized as the base swinging about the upper root of B_1, putting B_2 in compression [see Fig. 3(b)]. As described previously, rope B_2 (and the blade it represents) will buckle under any appreciable compressive load, causing massive stresses to appear in B_2 [see Fig. 3(c)]. As such, $|\phi| > \theta$, which we call "loading outside the blades," represents a region of instability for the x-pivot.

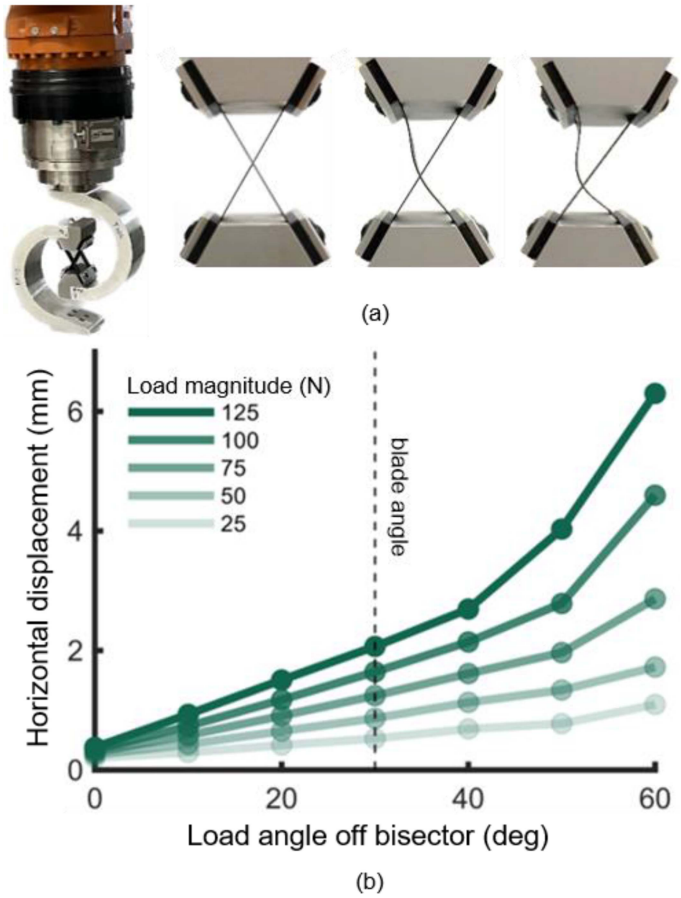

Fig. 4. (a) Experimental photos showing robotic tests and setup (left) and progressive buckling as a load of 125 N is applied at 0°, 40°, and 60° relative to the blade bisector (left to right). (b) Horizontal displacement of the free stage plotted as a function of load angle across various load magnitudes. For each load magnitude, buckling begins at the angle at which this relationship becomes nonlinear.

A similar instability occurs when the x-pivot is first locked in a rotated configuration, and then loaded in tension. In fact, there are many combinations of forces and moments that can produce this buckling behavior. Rather than attempting to enumerate every possible iteration of geometries, angles, applied forces, and applied moments that could lead to buckling, we encourage the reader to be alert to this possibility in any case of loading in tension at an angle relative to the grounded body.

This buckling phenomenon was validated by our benchtop experiments [see Fig. 4(a)]. For each tensile load, our measurements show a nonlinearity between horizontal displacement of the stage and load angle [see Fig. 4(b)]. The transition to this nonlinearity in each case corresponds to the onset of buckling in one of the blades. As load magnitude increased, the load angle associated with buckling approached the blade angle of the mechanism.

2) Designing to Avoid Buckling of X-Pivot Beams: We propose two design principles that can help avoid this buckling behavior. First, if the range of possible tensile loading directions is small and known, the x-pivot can be rotated in its plane such that the blade bisector is aligned with the predominant

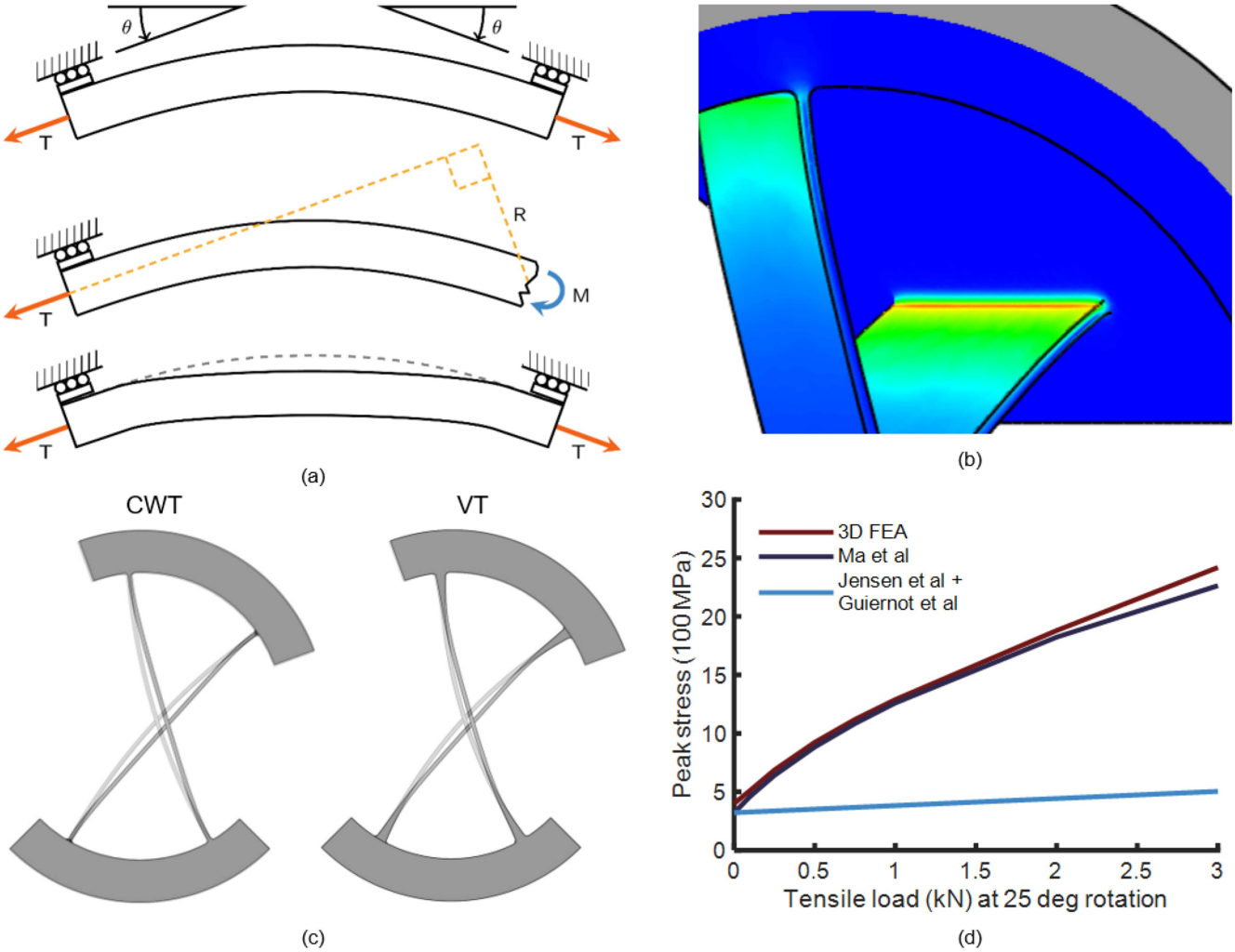

Fig. 5. (a) Illustrative model showing the combined loading effects that invalidate superposition-reliant models, and how those effects produce a characteristic bowstring shape. (b) 3-D FEA of the x-pivot beam under combined tension and angular deformation, with a narrow band of high stress at the crease. Stress values are represented on a color spectrum from blue (low stress) to red (high stress). (c) FEA-predicted beam deformation for constant width and thickness (CWT) and variable thickness (VT) blade types, under pure bending (background) and combined loading (foreground). The unique shape of the CWT blades under combined loading is the characteristic "bowstring" shape. (d) Peak stress under combined loading for the x-pivot under a fixed 25° angular deformation, as predicted by a superposition-reliant model, the 2-D FEA model, and 3-D FEA. .

tensile loading vector. Second, the angle of intersection of the blades (θ) can be increased, which would produce a larger range of potential loading directions "inside the blades," improving the design's robustness against buckling. It should be noted, however, that this second option would increase the stress in each blade during pure tension along the $\phi = 0$ vector, for simple trigonometric reasons; a larger angle between blade vectors and loading vector requires more tension in each "rope" to support the total load.

C. Nonsuperposition and Bowstringing

1) Problem: Combined Tension and Bending Invalidates Superposition-Reliant Models and Produces "Bowstring" Deformation: We now consider the case of "combined loading" for an x-pivot, meaning that the x-pivot is constrained to a fixed angular displacement and a force is applied normal to the x-pivot bases, as shown in Fig. 1(a). To build some intuition before examining the 3-D elastic solution in this scenario, we first appeal to the simplified model of a single beam in combined bending and tension, as shown in Fig. 5(a), top. In this simplified setting, it is clear that the applied angular displacement produces a bending moment throughout the beam, as would be the case in bending without a tensile force. Separately, the applied tensile force produces axial stress, as would be the case in tension without bending. However, the elastic solution in combined loading is not the sum of these parts: the bending and tension interact to produce an additional bending moment in the beam (force T acting on moment arm R) that is, to first order, the product of the applied axial force and the applied bending angle, as is shown in Fig. 5(a), middle. This interaction moment is maximal near the roots of the beam, producing a characteristic deformed shape, which we refer to as "bowstring" deformation [shown in Fig. 4(a), bottom].

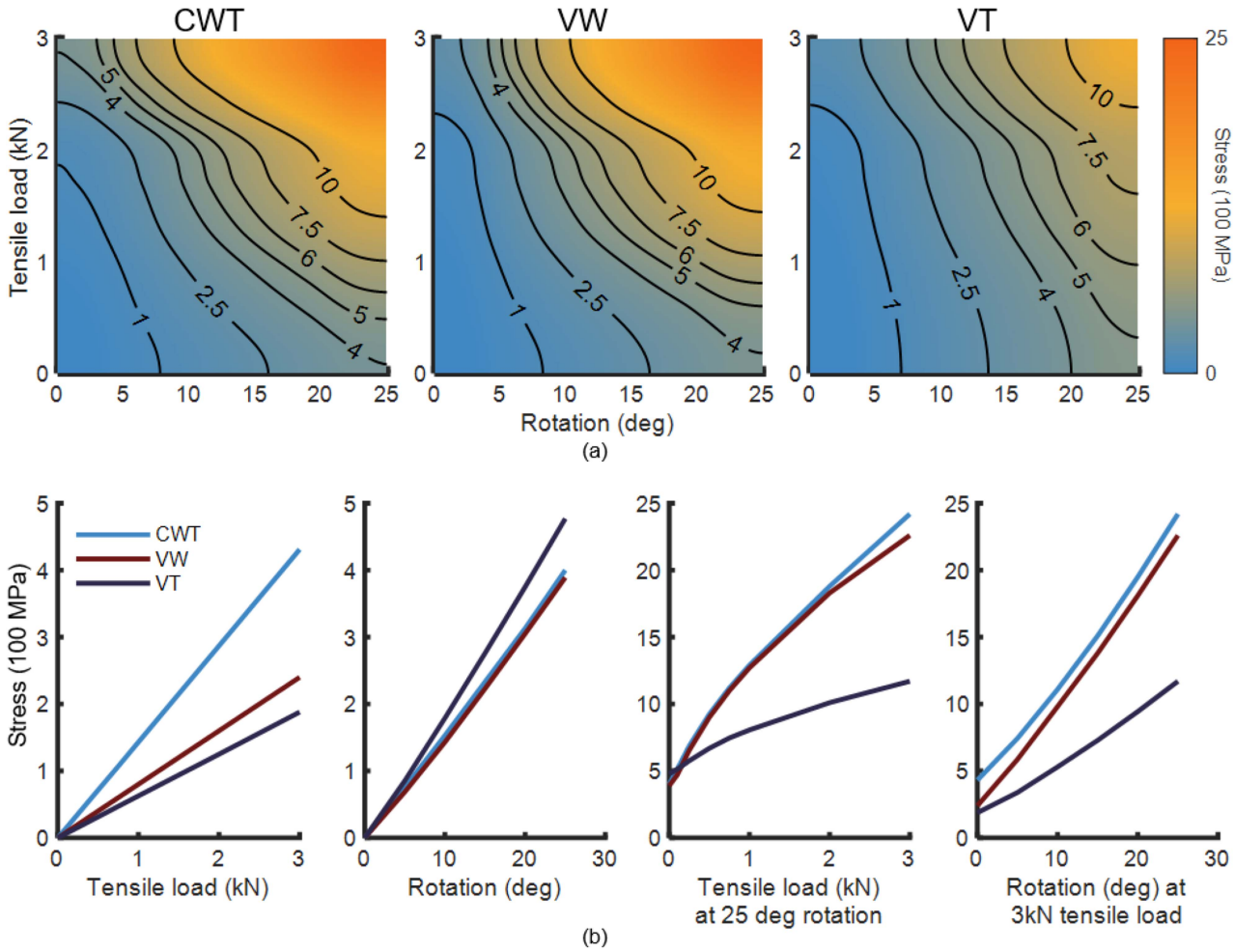

Fig. 6. (a) Stress as a function of tensile load and rotation (angular displacement) for constant width and thickness (CWT), variable width (VW), and variable thickness (VT) blade types. (b) Stress versus tensile load or rotation for pure tension, pure bending, and combined loading cases. Note that the lines on these plots represent cross-sectional cuts taken from the four outer edges of the contour plots in (a). From these plots, it is clear that the VT and VW blades perform well in tension, all three blade types have similar performance in rotation (with the VT blades being slightly worse), and the VT blades perform radically better in combined loading.

One implication of this observation is that models for combined loading that depend on superposition of solutions for normal and rotational loading can produce errors large enough to be of engineering importance. This is shown in Fig. 5(d). As before, we recommend the use of higher order modeling techniques such as Ma [28], Bilancia [25], or 3-D FEA to ensure that bowstring deformation is captured in the design process.

We have observed bowstring deformation in 3-D x-pivot models with constant width and thickness blades, as shown in Fig. 5(c). The accumulation of bending moment at the blade roots is associated with dramatic stress concentrations in the crease between the blade and body, shown in Fig. 5(b). The exact placement of this stress concentration can be slightly shifted by the presence of fillets in the crease, but with or without a small fillet, this stress concentration remains the dominant stress-driven design feature in combined loading.

2) Mitigating Bowstring Deformation in Combined Loading: One means of mitigating these effects in combined loading is to manipulate the beam geometry of the blade. Specifically, we explored three blade types as follows:

1) *Constant Width and Thickness (CWT):* Each blade has a constant rectangular cross-section along its length.
2) *Variable Width (VW):* Each blade has a rectangular cross section, with a *width* that changes along the beam's length. The blades are widest at their ends, and narrowest in the middle. This can also be thought of as a large-radius elliptical fillet along the blade's width.
3) *Variable Thickness (VT):* Each blade has a rectangular cross section, with a *thickness* that changes along the beam's length. The blades are thickest at their ends, and thinnest in the middle.

Note that all three beam types have small-radius fillets at the creases where the beams attach to the fixture at each end, to ease isolated stress concentrations that would otherwise develop at those creases.

When designing complex machines, bearing selection is often driven by lifetime/fatigue analysis. In a fatigue-oriented design

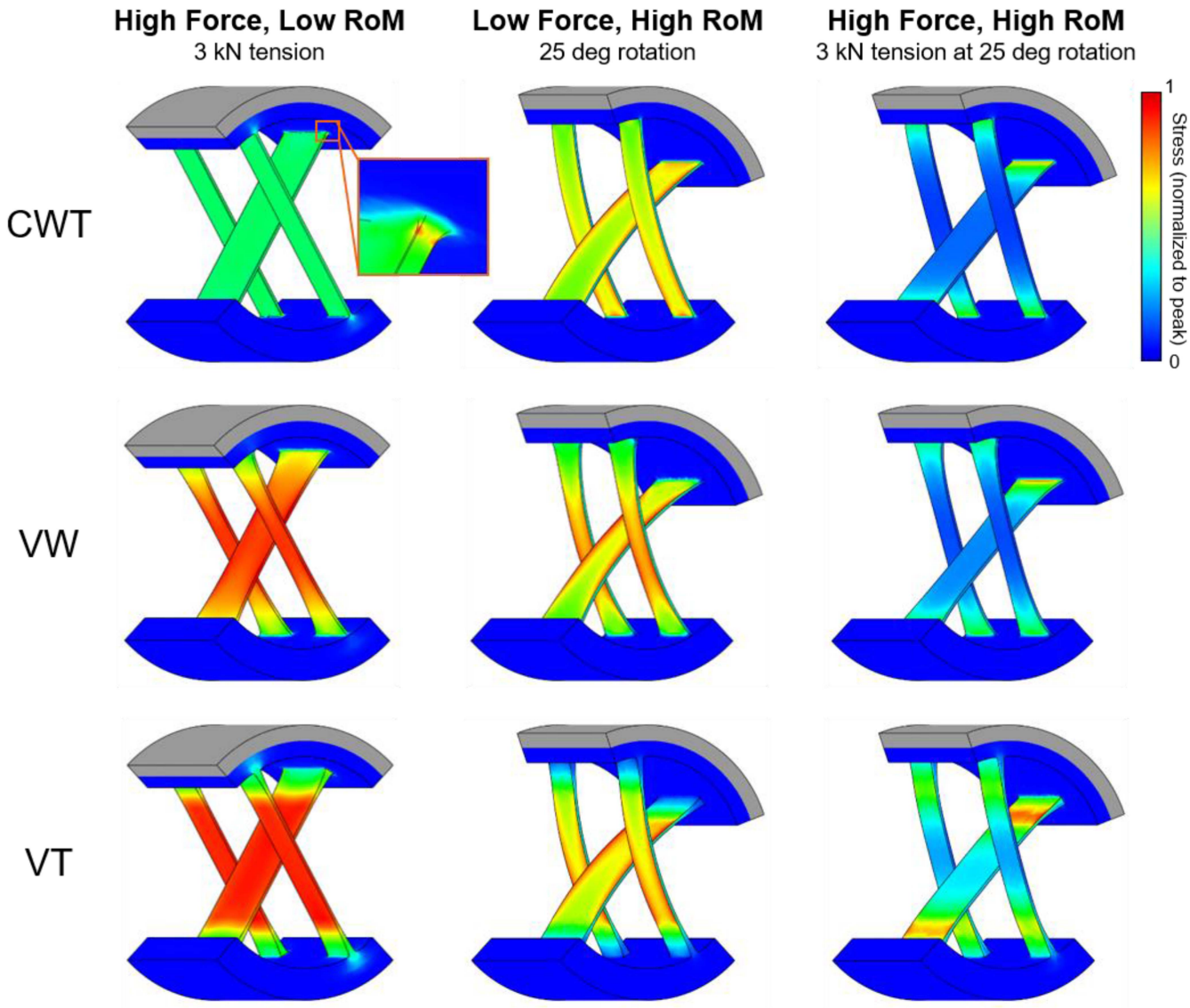

Fig. 7. 3-D FEA results from each of the three blade types in pure tension, pure rotation, and combined loading cases. Color maps for each blade type and loading condition are normalized to the peak stress for that type and condition. As such, these renderings are not intended for cross-type or cross-condition comparisons (for that we refer the reader to Fig. 5); rather they illustrate the distribution of stress *within* each blade type for a given loading condition.

approach, the decision of which beam type to use will be largely dependent on maximum stress under the expected loading conditions and desired range of motion (RoM). Indeed, we found that the blade types perform differently in each loading regime (see Table I).

a) High force, low RoM: In high force, low RoM applications, we found the VT blade to be the most effective (see Fig. 6). The variable thickness design diffuses what would otherwise be a stress concentration at the blade-body transition (the "crease"). We achieve a similarly smooth distribution of stress in the VW blade; however, for a space-constrained application with fixed total width, the VW design requires giving up some of the blade width at the midsections, which reduces the cross-sectional area available to support tensile loads. The CWT blades concentrate all of the stresses in the small crease fillet at the blade-body interface [see Figs. 5(b) and 7], leading to dramatically higher peak stress.

b) Low force, high RoM: In low force, high RoM applications, we found the CWT and VW blades to be almost equally effective (see Fig. 6). We do see a subtle decrease in peak stress in the VW blade, which can be attributed to distribution of the crease stresses across more material. In the VT blade, the increased thickness of a portion of the blade *decreases* the effective blade length in bending, which creates higher stresses for a given angular displacement (see Fig. 7).

c) High force, high RoM: In high force, high RoM applications, the VT blade is dramatically more effective than the other beam types (see Fig. 6). This is achieved by grading the flexural rigidity of the beam—making the base of the beam (where bowstring deformation would concentrate strain) more

TABLE I
LOADING REGIMES AND BLADE TYPES PERFORMANCE AS COMPARED TO CWT BLADES (BASELINE, OR "0")

	Low Force, High RoM	High Force, Low RoM	High Force, High RoM
CWT	0	0	0
VW	0	+	+
VT	- -	++	+++

Note: Number of "+" indicates improved performance, and number of "-" indicates reduced performance.

rigid than the middle of the beam, with a smooth transition in-between [see Fig. 5(c)]. This gradation of local flexural rigidity smoothly redistributes bending strain (and stress) more evenly along the blade length and away from the blade base (see Fig. 7).

Elaborating, the flexural rigidity of a beam such as the x-pivot blade is the product of the beam's material stiffness (Young's modulus) and the second moment of area of the beam about the bending axis. In the case of a beam with a rectangular cross section, such as the x-pivot blades, the second moment of area of the beam is *cubic* with respect to the beam thickness. Assuming that the blade is materially homogeneous, this cubic relationship makes thickness modulation an efficient method for locally modifying flexural rigidity (that is, a little added thickness goes a long way toward making the beam stiffer).

These principles were validated in our benchtop experiments, in which we compared 3-D-printed x-pivots with CWT and VT blades [see Fig. 8(a)]. Under high force, high RoM (4 kg at 30°), the VT mechanism dramatically reduced bowstringing, distributing curvature (and hence, stress) more evenly along its blade length compared to the CWT mechanism [see Fig. 8(b)]. These data follow the trends shown in the analogous FEA data in Fig. 6(b) (third plot from left). In the low force, high RoM condition (0.5 kg at 30°), we observed higher normalized curvatures in the VT blade than the CWT blade, consistent with our FEA findings. Note that the VT mechanism was stiffer than the CWT mechanism, and so did not reach the full 30° rotation in the low load case.

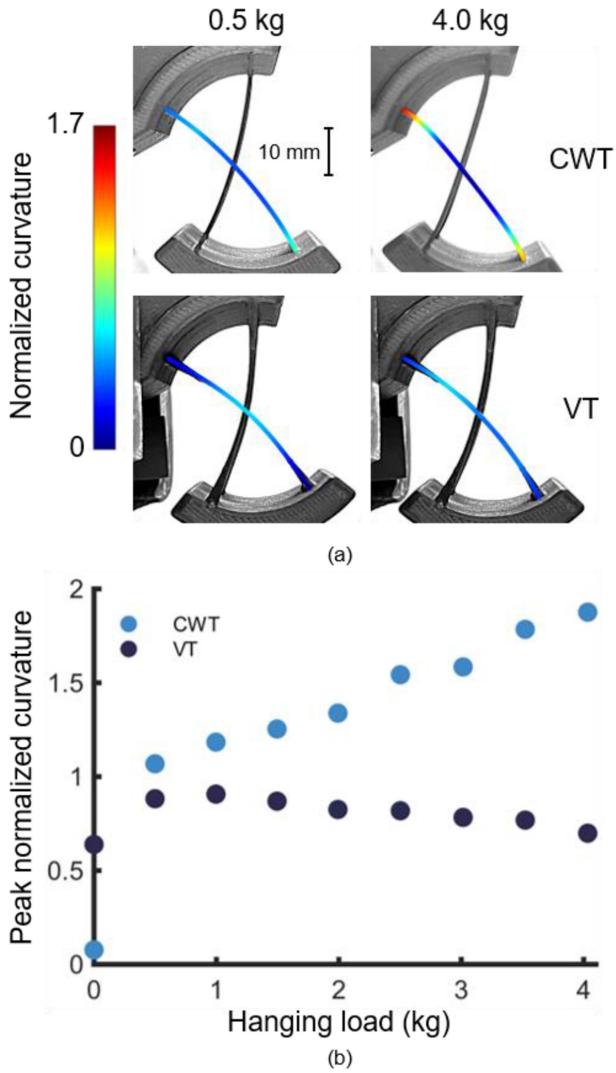

Fig. 8. (a) Experimental photos comparing blade curvature between CWT and VT mechanisms loaded at 30°. Normalized curvature values at each point are presented as blade length/radius of curvature. (b) Peak normalized curvature from the two blade types under increasing loads, all at 30°.

IV. DESIGN CONSIDERATIONS OTHER THAN STRESS

A. Manufacturability

The precision required of compliant mechanisms can make them extremely difficult and expensive to fabricate. We have found that such manufacturing constraints can be obtrusive enough to outweigh the potential benefits of any given design improvement. For instance, increasing the number of blades across the mechanism width to reduce anticlastic effects becomes infeasible well before the blades become narrow enough to be beam-like. The design consideration with perhaps the most pronounced impact on manufacturability is selection of blade type. Theoretically, the CWT and VW blades should be the easiest to manufacture in isolation, as their constant thickness allows them to be cut from rolled shim stock. These shim blades could then be affixed to the x-pivot's base via bolts, welds, or interlocking components. In practice, however, this makes the "crease fillets" difficult to realize, and could potentially lead to stress risers where blade meets base.

The VW blades do have a continuous nonlinear planar geometry, which would likely require a CNC machine or specialized jig to cut. We expect that the VT blades would be more difficult to manufacture than the other blade types, because the thickness variation would likely require precision machining. That

said, our results show that the benefits provided by VT blades may well be worth the added manufacturing effort in cases of combined loading.

B. Compactness

The overall size of the mechanism can also weigh heavily in guiding design decisions. For instance, although higher blade angles provide greater robustness to variations in loading vector direction, they also typically increase the footprint of both bases, which must be widened to accommodate the shallower blade slope. Volume constraints also play a poignant role in blade-type selection. In a width-limited setting, the constant width blades (CWT and VT) make full use of available width for the blade. This is important because the strength of the flexure in tension is theoretically limited by the beams' smallest cross sections; given that RoM is inversely related to blade thickness, the most obvious way to improve tensile strength is to maximize blade width. In practice, we found that maximum stress tends to be dictated instead by stress concentrations at the corners of the blades. VW blades provide a means of distributing these stresses without changing blade thickness, and thereby increasing bending stress. The overall flexure geometry allows the curved profiles of the VW blades to be nested in such a way that they only effectively increase each blade width by the width added to one of the blades (e.g., ½ of the added width for a 2-blade x-pivot, ⅓ of the added width for a 3-blade x-pivot, etc.). This nesting feature helps to offset the geometric penalty associated with the VW blades, and may make them an appropriate option for relatively low-RoM, high-tension applications.

V. Conclusion

Of all compliant mechanism architectures with the ability to constrain motion in every direction except rotation about a single axis, x-pivots are perhaps the most important to real-world mechatronic systems. The principles established in this article provide a foundation for informed stress-based design of x-pivots that will withstand realistic loading conditions. It is our hope that this work will facilitate the incorporation of compliant mechanisms into future mechatronic devices, thereby reducing component wear and improving system longevity.

Acknowledgment

The employee owns all right, title and interest in and to the article and is solely responsible for its contents. The United States Government retains and the publisher, by accepting the article for publication, acknowledges that the United States Government retains a non-exclusive, paid-up, irrevocable, worldwide license to publish or reproduce the published form of this article or allow others to do so, for United States Government purposes. The DOE will provide public access to these results of federally sponsored research in accordance with the DOE Public Access Plan https://www.energy.gov/downloads/doe-public-access-plan.

References

[1] L. L. Howell, *Compliant Mechanisms*. Hoboken, NJ, USA: Wiley, 2001.
[2] J. B. Hopkins and M. L. Culpepper, "Synthesis of multi-degree of freedom, parallel flexure system concepts via freedom and constraint topology (FACT)–Part I: Principles," *Precis. Eng.*, vol. 34, no. 2, pp. 259–270, 2010, doi: 10.1016/j.precisioneng.2009.06.008.
[3] J. B. Hopkins and M. L. Culpepper, "Synthesis of multi-degree of freedom, parallel flexure system concepts via freedom and constraint topology (FACT). Part II: Practice," *Precis. Eng.*, vol. 34, no. 2, pp. 271–278, 2010, doi: 10.1016/j.precisioneng.2009.06.007.
[4] J. B. Hopkins, "Design of parallel flexure systems via freedom and constraint topologies (FACT)," master's thesis, MIT, Cambridge, MA, USA, 2010.
[5] P. A. Halverson, L. L. Howell, and A. E. Bowden, "A flexure-based biaxial contact-aided compliant mechanism for spinal arthroplasty," in *Proc. ASME Int. Des. Eng. Tech. Conferences Comput. Inf. Eng. Conf.*, 2008, vol. 2, pp. 405–416, doi: 10.1115/DETC2008-50121.
[6] C. B. Pedersen, T. Buhl, and O. Sigmund, "Topology synthesis of large-displacement compliant mechanisms," *Int. J. Numer. Methods Eng.*, vol. 50, no. 12, pp. 2683–2705, 2001.
[7] E. R. Homer et al., "New methods for developing and manufacturing compliant mechanisms utilizing bulk metallic glass," *Adv. Eng. Mater.*, vol. 16, no. 7, pp. 850–856, 2014, doi: 10.1002/adem.201300566.
[8] M. Xun, H. Yu, Y. Liu, J. Deng, S. Zhang, and K. Li, "A precise rotary piezoelectric actuator based on the spatial screw compliant mechanism," *IEEE/ASME Trans. Mechatron.*, vol. 28, no. 1, pp. 223–232, Feb. 2023.
[9] K. Xu and H. Liu, "Design of a compliant flapping-wing mechanism with flapping–twist–swing motion," *IEEE/ASME Trans. Mechatron.*, vol. 27, no. 6, pp. 5197–5207, Dec. 2022.
[10] J. Bastien and L. Birglen, "Power efficient design a compliant robotic leg based on Klann's linkage," *IEEE/ASME Trans. Mechatron.*, vol. 28, no. 2, pp. 814–824, Apr. 2023.
[11] W. E. Young, "An investigation of the cross-spring pivot," *J. Appl. Mech.*, vol. 11, pp. A113–A120, 1944.
[12] J. A. Haringx, "The cross-spring pivot as a constructional element," *Appl. Sci. Res.*, vol. 1, 1949, Art. no. 313.
[13] A. E. Guérinot, S. P. Magleby, and L. L. Howell, "Preliminary design concepts for compliant mechanism prosthetic knee joints," in *Proc. ASME Des. Eng. Tech. Conf.*, 2004, vol. 2 B, pp. 1103–1111, doi: 10.1115/detc2004-57416.
[14] J. Dearden, C. Grames, J. Orr, B. D. Jensen, S. P. Magleby, and L. L. Howell, "Cylindrical cross-axis flexural pivots," *Precis. Eng.*, vol. 51, pp. 604–613, 2018, doi: 10.1016/j.precisioneng.2017.11.001.
[15] P. Bilancia, M. Baggetta, G. Berselli, L. Bruzzone, and P. Fanghella, "Design of a bio-inspired contact-aided compliant wrist," *Robot. Comput.-Integr. Manuf.*, vol. 67, 2021, Art. no. 102028, doi: 10.1016/j.rcim.2020.102028.
[16] P. P. Valentini and E. Pezzuti, "Design and interactive simulation of cross-axis compliant pivot using dynamic splines," *Int. J. Interactive Des. Manuf.*, vol. 7, no. 4, pp. 261–269, 2013, doi: 10.1007/s12008-012-0180-x.
[17] Y. Chen, M. Yang, D. Wu, Z. Du, and W. Dong, "Static modeling of a cross-spring flexure pivot with variable cross-section," in *Proc. Int. Symp. Flexible Automat.*, 2018, pp. 25–29.
[18] R. M. Panas, F. Sun, L. Bekker, and J. B. Hopkins, "Combining cross-pivot flexures to generate improved kinematically equivalent flexure systems," *Precis. Eng.*, vol. 72, pp. 237–249, 2021, doi: 10.1016/j.precisioneng.2021.05.001.
[19] A. E. Guérinot, S. P. Magleby, L. L. Howell, and R. H. Todd, "Compliant joint design principles for high compressive load situations," *J. Mech. Des.*, vol. 127, no. 4, pp. 774–781, Aug. 2005, doi: 10.1115/1.1862677.
[20] W. K. Yu and T. A. Harris, "A new stress-based fatigue life model for ball bearings," *Tribol. Trans.*, vol. 44, no. 1, pp. 11–18, 2001, doi: 10.1080/10402000108982420.
[21] A. Harnoy, *Bearing Design in Machinery*. New York, NY, USA: Marcel Dekker, 2002.
[22] T. E. Tallian, "Simplified contact fatigue life prediction model-part I: Review of published models," *J. Tribol.*, vol. 114, no. 2, pp. 207–213, 1992, doi: 10.1115/1.2920875.
[23] B. D. Jensen and L. L. Howell, "The modeling of cross-axis flexural pivots," *Mech. Mach. Theory*, vol. 37, no. 5, pp. 461–476, 2002, doi: 10.1016/S0094-114X(02)00007-1.
[24] P. Bilancia and G. Berselli, "An overview of procedures and tools for designing nonstandard beam-based compliant mechanisms," *CAD Comput. Aided Des.*, vol. 134, 2021, Art. no. 103001, doi: 10.1016/j.cad.2021.103001.

[25] P. Bilancia, M. Baggetta, G. Hao, and G. Berselli, "A variable section beams based Bi-BCM formulation for the kinetostatic analysis of cross-axis flexural pivots," *Int. J. Mech. Sci.*, vol. 205, 2021, Art. no. 106587, doi: 10.1016/j.ijmecsci.2021.106587.
[26] P. Bilancia, G. Berselli, S. Magleby, and L. Howell, "On the modeling of a contact-aided cross-axis flexural pivot," *Mech. Mach. Theory*, vol. 143, Jan. 2020, Art. no, 103618, doi: 10.1016/j.mechmachtheory.2019.103618.
[27] S. Li, G. Hao, Y. Chen, J. Zhu, and G. Berselli, "Nonlinear analysis of a class of inversion-based compliant cross-spring pivots," *J. Mech. Robot.*, vol. 14, no. 3, Jun. 2022, Art. no. 031007, doi: 10.1115/1.4052514.
[28] F. Ma and G. Chen, "Modeling large planar deflections of flexible beams in compliant mechanisms using chained beam-constraint-model," *J. Mech. Robot.*, vol. 8, no. 2, May 2016, Art. no. 021018, doi: 10.1115/1.4031028.
[29] S. P. Timoshenko and J. N. Goodier, *Theory of Elasticity*. New York, NY, USA: McGraw-Hill, 1934.
[30] S. Suresh, *Fatigue of Materials*. Cambridge, U.K.: Cambridge Univ. Press, 1998.
[31] L. Euler, *Methodus Inveniendi Lineas Curvas… Sive Solutio Problematis Isoperimetrici. (Cum Tabulis Aeneis).* Belchertown, MA, USA: Marcus-Michael Bousquet, 1744.

Brandon T. Peterson (Member, IEEE) received the B.S. degree in computer engineering in 2017 and the B.A. degree in mathematics from the University of Florida, Gainesville, FL, USA, and the M.S. degree in robotics from the University of Michigan, Ann Arbor, MI, USA, in 2019. He is currently working toward the Ph.D. degree in the Department of Mechanical and Aerospace Engineering, University of California, Los Angeles, Los Angeles, CA, USA.

Thomas J. Hardin received the B.S. degree in mathematics and the B.S. and M.S. degrees in mechanical engineering from Brigham Young University, Provo, UT, USA, in 2012 and 2014, respectively, and the Ph.D. degree in materials science from the Massachusetts Institute of Technology, Cambridge, MA, USA, in 2018.

He is currently a Senior Member of the Technical Staff with the Material, Physical, and Chemical Sciences Center, Sandia National Laboratories, Albuquerque, NM, USA, and recently completed the President Harry S. Truman Fellowship in National Security Science and Engineering at Sandia National Laboratories. Dr. Hardin is a member of the American Ceramic Society, the Materials Research Society, and The Minerals, Metals and Materials Society.

Armin W. Pomeroy received the B.S. degree in mechanical engineering from the University of California, Los Angeles, CA, USA, in 2019. He is currently working toward the Ph.D. degree in the Department of Mechanical and Aerospace Engineering, University of California, Los Angeles, Los Angeles, CA, USA.

Jonathan B. Hopkins (Member, IEEE) received the B.S., M.S., and Ph.D. degrees from the Massachusetts Institute of Technology, Cambridge, MA, USA, in 2010, 2007, and 2005, respectively, all in mechanical engineering.

He is currently a Full Professor of Mechanical and Aerospace Engineering with the University of California, Los Angeles, CA, USA. His research interests include enabling the design and fabrication of flexible structures, mechanisms, and materials that achieve extraordinary capabilities via the deformation of their constituent compliant elements.

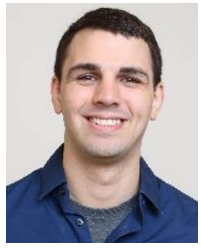

Tyler R. Clites received the B.S. degree in engineering sciences from Harvard College, Cambridge, MA, USA in 2014, and the Ph.D. degree in medical engineering and medical physics from the Health Sciences and Technology program, Massachusetts Institute of Technology, Cambridge, MA, USA, and Harvard Medical School, Boston, MA, in 2018.

He is currently an Assistant Professor of Mechanical and Aerospace Engineering, Bioengineering, and Orthopaedic Surgery with the University of California, Los Angeles, CA, USA. His research interests include the field of bionics, and more specifically anatomics, which he defines as co-engineering of body and machine in pursuit of improved human function.